Acoustic Velocity and Optical Index Birefringence in A-Plane ZnO Thin Films

Yi-Hsin Chen,[1] Yu-Chieh Wen,[1] Wei-Rein Liu,[2] Wen-Feng Hsieh,[2] and Chi-Kuang Sun[1,3,*]

[1]*Department of Electrical Engineering and Institute of Photonics and Optoelectronics, National Taiwan University, Taipei 10617, Taiwan*

[2]*Department of Photonics, National Chiao-Tung University, Hsinchu 30010, Taiwan*

[3]*Research Center for Applied Sciences, Academia Sinica, Taipei 115, Taiwan*

(Received April 12, 2010)

The longitudinal acoustic velocity in the direction normal to the c-axis and the birefringence of refractive index of a-plane zinc oxide (ZnO) thin films were measured by ultrafast transient reflection measurement. Through Fourier analysis, the experimental data show that the acoustic velocity is about 6000 m/s and the measured refractive index near the band gap, which is higher than the previously reported results by 20 $\sim$ 30%.

PACS numbers: 43.58.+z, 78.20.Ci

I. INTRODUCTION

Zinc oxide (ZnO) is a member of the II-VI semiconductors with a large direct bandgap ($\sim$3.4 eV), which makes ZnO a candidate material system for blue to ultraviolet light emitters [1–4]. Its outstanding piezoelectric property also makes it possible to fabricate optical piezoelectric transducer for nanoacoustic devices. Accurate knowledge of its acoustic velocity and optical refractive index is essential for the design of acoustic devices. Although there have been many reports the refractive index of ZnO, the value of refractive index near the bandgap is inconsistent between different works [1–3]. The most common technique for measuring the refractive index of semiconductor thin films is ellipsometry. Since it is an indirect methodobtain the refractive index from the measured raw data relies on accurate understanding of sample conditions such as roughness. In this study, we use ultrafast transient reflection measurement, which is a simpler and more direct method, to measure the longitudinal acoustic velocity in the direction normal to the c-axis and the birefringence of refractive index of high-quality a-plane ZnO thin films through backward Brillouin scattering. By Fourier analysis, the experimental data show that the longitudinal acoustic velocity in the direction normal to the c-axis is about 6000 m/s and the measured refractive index near the bandgap is 20 $\sim$ 30% times higher than previous reports.

II. METHOD

II-1. Generation of coherent acoustic phonons (CAPs)

In this study, we used ultrafast pump probe technique to generate and detect the coherent longitudinal acoustic (LA) phonons. [5–7] The schematic is shown in FIG. 1. A

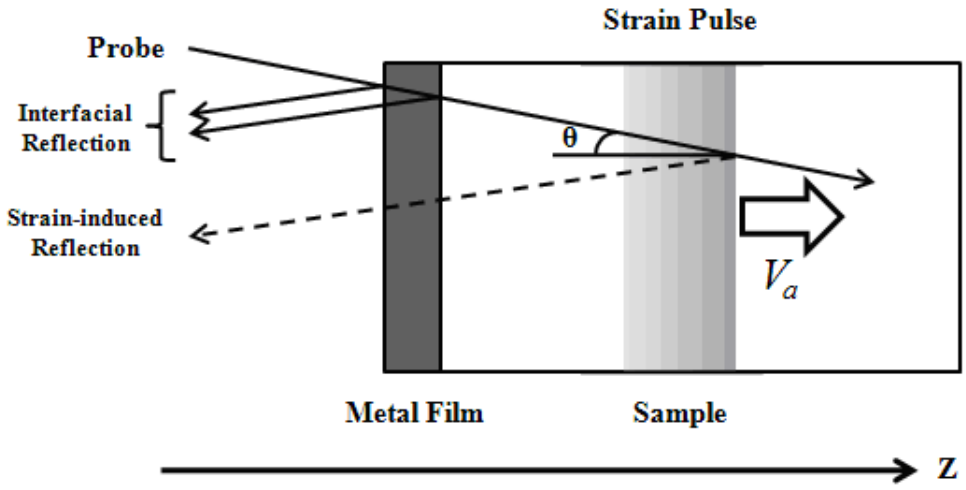

FIG. 1: Schematic diagram of the backward Brillouin scattering.

pump beam with a pulse duration of about 200 fs was absorbed by the metal film deposited on the surface of the sample. The generation of coherent acoustic phonons was achieved by the thermal expansion of the metal film. Since the skin depth of the metal is on the scale of only a few nanometers and the illuminated area (spot size of pump) is typically a few tens of microns, we can only consider the excitation of longitudinal acoustic phonons. [5–10] The generated strain pulses propagated in the lower case direction and bounced back. At the metal-sample interface, the reflection coefficient r_{ac} is

$$r_{ac} = (Z_s - Z_f)/(Z_s + Z_f), \tag{1}$$

where Z_s and Z_f are the acoustic impedances of the sample under test and the metal film, respectively. At the free surface, the reflection coefficient is -1. The central wavelength λ' of the transmitted strain pulse into the sample can be estimated by [5]

$$\lambda' \sim d(V_s/V_f), \tag{2}$$

where d is the thickness of the metal film, and V_s and V_f are the longitudinal acoustic velocity of the sample and the metal film, respectively.

II-2. Detection of CAPs

The generated strain pulse propagated in the sample under study with a longitudinal acoustic velocity V_s. To detect the propagating strain pulse, we used a probe beam, which had a time delay t relative to the pump beam. The probe beam was reflected at the air-metal interface and metal-sample interface (interfacial reflection), as shown in FIG. 1. There was an additional reflection (strain-induced reflection) because the strain pulse induced a local change δn in the refractive index. We imagined the situation as one in which a strain-induced mirror moved at V_s that reflected the probe beam. Since the mirror

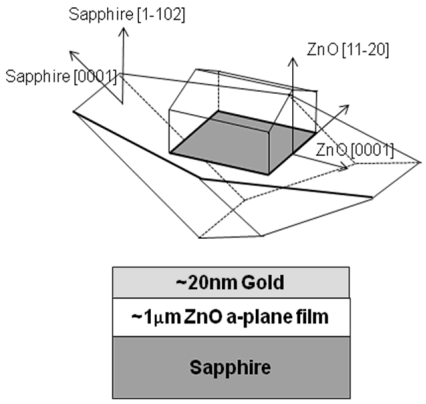

FIG. 2: The upper shows the crystal orientation of the sample. The lower is the cross-section of the sample.

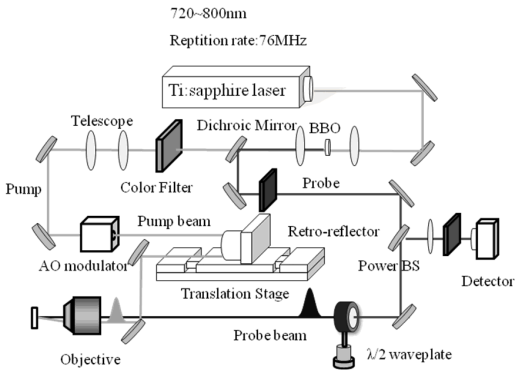

FIG. 3: Schematic diagram of the experimental setup.

was moving, the phase difference between the interfacial reflection and the strain-induced reflection changed periodically from 0 to 2π. Therefore, the total reflection of probe was oscillatory in time. The period of the oscillation T can be described by the following relation [7]:

$$T = \frac{\lambda}{2nV_s \cos\theta}, \tag{3}$$

where n is the refractive index of the sample seen by the probe, θ is the angle of the probe inside the sample, and λ is the wavelength of the probe.

III. EXPERIMENTAL SETUP

Sample under study is a wurzite a-plane thin film with a thickness about 1 μm grown on a r-plane sapphire substrate by pulsed laser deposition and was coated with a 18-nm-thick gold film as the transducer for pulsed acoustic wave generation. The sample structure is shown in FIG. 2.

To measure the acoustic velocity and refractive index, we investigated the backward Brillouin scattering mentioned in section II through two-color pump probe transient measurement. A Ti:sapphire laser was used to generate linearly polarized femtosecond pulses with a repetition rate of 76-MHz in the wavelength range from 720 to 800 nm. By focusing the laser beam on a 0.5-mm-thick BBO, the optical frequency was doubled. We used a dichroic beamsplitter to separate the fundamental component (720∼800 nm) as the pump beam and the second harmonic component (360∼400 nm) as the probe beam. By using a half-wave plate to control the polarization of the probe beam, we can measure the birefringence of the sample. The setup was configured to ensure that the probe beam was normally incident to the sample. The experimental setup is shown in FIG. 3.

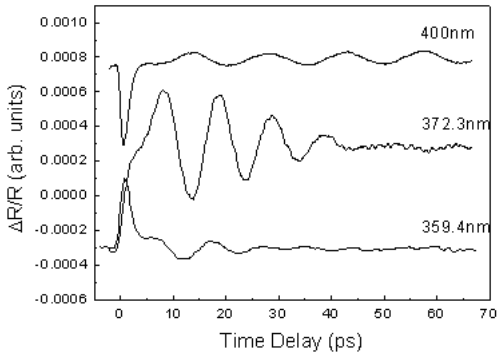

FIG. 4: The measured traces at different wavelength as the polarization of probe is normal to the c-axis of ZnO.

IV. RESULTS AND DISCUSSION

We first measured the sample by the probe whose polarization is normal to the c-axis at different central wavelengths (400 nm, 390 nm, 385 nm, 380.1 nm, 375.3 nm, 372.3 nm, 369.1 nm, 367 nm, 364 nm, and 359.4 nm). FIG. 4 shows the experimental results of the measured transient reflection with 359.4-nm, 372.3-nm and 400-nm probe wavelengths. We can observe that the oscillation attenuates rapidly when the photon energy of the probe is near or above the bandgap of ZnO. This is due to the strong absorption of the probe near the bandgap. We took this attenuation effect into consideration and performed the Fourier analysis to resolve the oscillation frequency at different probe wavelengths. From Eq. (3), we can obtain the product of refractive index n and longitudinal acoustic velocity V_a from the oscillation frequency of the backward Brillouin scattering. Once we know the value of the refractive index, we can calculate the value of the longitudinal acoustic velocity, and vice versa. From the previous works [1–3], the value of refractive index of ZnO at photon energy far below the bandgap are sample-independent. Here, we used $n = 2.27$ at 400 nm from the work of H. Yoshikawa *et al.* [1] as the reference value. With the oscillation frequency measured by the 400-nm-probe, which is 68.9 GHz, $n = 2.27$, $\theta = 0°$ (normal incident), and $\lambda = 400$ nm, we recovered the value of longitudinal acoustic velocity in the direction normal to c-axis, which is 6070 ± 150 m/s. This result is quite consistent with the previous works [11, 12]. By using a pump with photon energy far below the bandgap of ZnO, we can reasonably assume that the pump does nothing to the sample, except generating coherent LA phonons through the metal film. Therefore, the acoustic velocity should be the same in the wavelength region of our experiment. We can then use the value of the recovered longitudinal acoustic velocity to measure the refractive index at other wavelengths. Then we paralleled the polarization of the probe to the c-axis and repeated the same procedures as above. The measured oscillation frequencies and the deduced refractive indices at different probe wavelengths and different probe polarizations are shown in TABLE I.

TABLE I: The measured oscillation frequency and the deduced refractive index

	E∥c		**E⊥c**	
Wavelength of probe	Oscillation frequency	Refractive index	Oscillation frequency	Refractive index
(nm)	(GHz)	(n_e)	(GHz)	(n_o)
400	68.9	2.27	68.8	2.27
390	75.1	2.41	71.7	2.31
385	74.6	2.37	75.6	2.40
380.1	78.6	2.46	78.6	2.46
375.3	82.7	2.56	86.3	2.67
372.3	88.8	2.72	94.8	2.91
369.1	92.4	2.81	94.2	2.87
367	94.2	2.85	90.1	2.73
364	91.3	2.74	85.1	2.56
359.4	86.4	2.56	86.0	2.55

The measured refractive index birefringence is summarized in FIG. 5, and compared with that from H. Yoshikawa *et al.* [1]. We can observe that the trend of our result and that of Yoshikawa *et al.* are similar: the ordinary and extraordinary refractive indices change sharply near the bandgap, but the resonance peak of the extraordinary refractive index shifts to a high photon energy. This is attributed to the electronic band structure of ZnO [13]. As the literature states [13], the conduction band (CB) of ZnO has symmetry Γ_7 and the valence band (VB) is split into three sub-VBs named AΓ_7, BΓ_9, and CΓ_7 under the influence of the hexagonal crystal field and the spin-orbit interaction. Selection rules allow transitions from the two upper AΓ_7 and BΓ_9 VBs to the Γ_7 CB only for $\mathbf{E}\perp\mathbf{c}$ (ordinary) and transitions from CΓ_7 VB to Γ_7 CB only for $\mathbf{E}\|\mathbf{c}$ (extraordinary); so the resonance (extraordinary), resulting in peak of extraordinary refractive index at a high photon energy. We also observe that at the vicinity of the bandgap, the refractive index from our results is $20 \sim 30\%$ times higher than that from H. Yoshikawa *et al.* Ref. [1]. We infer that this is due to the better quality of our sample by the following reasons. ZnO has a large exciton binding energy (60 meV); so the excitonic effects are significant even at room temperature. R. J. Elliott [14] and C. Tanguy [15] proposed that the Wannier excitons will enhance the optical absorption when the photon energy is near the bandgap. This is called the excitonic effect, and hence it will result in a resonance peak in the refractive index. A direct bandgap crystal (as ZnO) with a worse quality (more defects) will induce a larger broadening Γ for the direct interband transition than that for a crystal with a better quality (less defects), and thus smear out the resonance peaks near the bandgap, as stated in the paper of C. Tanguy [15]. In [1], H. Yoshikawa *et al.* considered three contributions to the dielectric constant $\varepsilon = \varepsilon_1 + i\varepsilon_2$: the one-electron contribution, the discrete-exciton contribution, and the continuum-exciton contribution. These contributions were described by the following

equations. For the one-electron contribution [1],

$$\varepsilon(E) = \sum_{\alpha=A,B,C} A_{0\alpha} E_{0\alpha}^{-1.5} f(\chi_{0\alpha}), \tag{4}$$

$$A_{0\alpha} = \frac{4}{3}\left(\frac{3}{2}\mu_{0\alpha}\right)^{1.5} P_{0\alpha}^2, \tag{5}$$

$$\chi_{0\alpha} = \big(E + i\Gamma\big)/E_{0\alpha}, \tag{6}$$

$$f(\chi_{0\alpha}) = \chi_{0\alpha}^{-2}\big[2 - (1+\chi_{0\alpha})^{1/2} - (1-\chi_{0\alpha})^{1/2}\big], \tag{7}$$

where $\mu_{0\alpha}$ is the combined density-of-states mass, $P_{0\alpha}^2$ is the squared momentum-matrix element, Γ is the broadening, $E_{0\alpha}$ is the energy gap and α (= A, B, C) denotes the $A\Gamma_7 \to \Gamma_7$, $B\Gamma_9 \to \Gamma_7$, and $C\Gamma_7 \to \Gamma_7$ transitions, respectively. For the discrete-exciton contribution [1],

$$\varepsilon(E) = \sum_{\alpha=A,B,C} \sum_{n=1}^{\infty} \frac{A_{0x}^{n\alpha}}{E_{0x}^{n\alpha} - E - i\Gamma}, \tag{8}$$

$$E_{0x}^{n\alpha} = E_{0\alpha} - G_{0\alpha}^{3D}/n^2, \tag{9}$$

where $A_{0x}^{n\alpha}$ is the discrete-exciton strength parameter, $E_{0\alpha}^{n\alpha}$ is the discrete-exciton energy, and $G_{0\alpha}^{3D}$ is the 3D-exciton Rydberg energy. For the continuum-exciton contribution [1],

$$\varepsilon(E) = \sum_{\alpha=A,B,C} \sum_{n=1}^{\infty} \frac{A_{0x}^{C\alpha} E_{0\alpha}^{C1}}{4G_{0\alpha}^{3D}(E+i\Gamma)^2} \ln \frac{E_{0\alpha}^2}{E_{0\alpha}^2 - (E+i\Gamma)^2}, \tag{10}$$

where $A_{0x}^{C\alpha}$ is the continuum-exciton strength parameter and $E_{0\alpha}^{C1}$ is the ground state exciton energy, which is approximately equal to $E_{0\alpha}$. The dielectric constant is the sum of Eqs. (4), (8), (10), and an additional term $\varepsilon_{1\infty}$, which arises from the higher-lying gap transitions. Further, the refractive index is calculated by

$$n(E) = \left(\frac{\big[\varepsilon_1(E)^2 + \varepsilon_2(E)^2\big]^{1/2} + \varepsilon_1(E)}{2}\right)^{1/2}. \tag{11}$$

We calculated the solid fitting line in FIG. 5 by the above equations and parameters in [1], but we chose a smaller broadening $\Gamma = 40$ meV (in [1], $\Gamma = 145$ meV); the parameters we used are shown in TABLE II. We see that the smaller the broadening Γ, the more apparent is the resonance peak. With these fitting results, the disagreement of our results with that in Ref. [1] near the bandgap can thus be attributed to the greatly improved

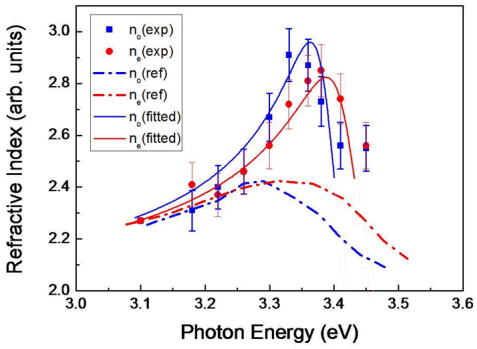

FIG. 5: The measured refractive index birefringence (solid squares for $n_{\rm o}$, and solid circles for $n_{\rm e}$). The blue represents $n_{\rm o}$, and the red represents $n_{\rm e}$. The dash-dot lines are results from Yoshikawa *et al.* The solid lines are calculated by the same model of Yoshikawa *et al.* [1], but with a smaller broadening (40meV).

TABLE II: Parameters used in the calculation of the solid fitting lines

Parameter	$\mathbf{E}\|\mathbf{c}$	$\mathbf{E}\perp\mathbf{c}$
E_{0A} (eV)	3.450	(forbidden)
E_{0B} (eV)	3.453	(forbidden)
E_{0C} (eV)	(forbidden)	3.484
$G_{0\alpha}^{3D}$ (meV)	59	59
A_{0A} (eV$^{1.5}$)	12.45	(forbidden)
A_{0B} (eV$^{1.5}$)	12.50	(forbidden)
A_{0C} (eV$^{1.5}$)	(forbidden)	24.90
A_{0x}^{1A} (eV)	0.13	(forbidden)
A_{0x}^{1B} (eV)	0.13	(forbidden)
A_{0x}^{1C} (eV)	(forbidden)	0.259
A_{0x}^{CA} (eV^2)	0.165	(forbidden)
A_{0x}^{CB} (eV^2)	0.164	(forbidden)
A_{0x}^{CC} (eV^2)	(forbidden)	0.329
Γ (meV)	40	40
$\varepsilon_{1\infty}$	2.09	2.18

quality of our sample. Comparing to the previous works, the reported values in this paper are much closer to the intrinsic values.

The method used here has a high potential for measuring the refractive index of samples with nanostructures than ellipsometry, because the ellipsometry measures the sample

as a whole: it has to take contributions from the whole sample into consideration. It is very difficult to build an appropriate model for the sample with nanostructures. However, in picoseconds ultrasonics, since we use the nano-strain pulse to probe the sample, from Eq. (2), we can measure the sample locally with resolution of about tens of nanometers (the wavelength of the strain field). This makes the analysis of experimental data much simpler.

V. CONCLUSIONS

In this paper, we reported the longitudinal acoustic velocity and refractive index birefringence of ZnO. The measured longitudinal acoustic velocity is about 6000 m/s, and the measured refractive index near the bandgap is 20 $\sim$ 30% higher than obtained in previous works due to the stronger intrinsic excitonic effect. We also have demonstrated a much simpler and more direct method to measure the refractive index, and we believe that it has a high potential to measure samples with nanostructures.

Acknowledgments

The ZnO sample was prepared by Wei-Rein Liu and Wen-Feng Hsieh. This work was supported by the National Science Council of Taiwan under grant number NSC 98-2120-M-002-001.

References

* Electronic address: sun@cc.ee.ntu.edu.tw

[1] H. Yoshikawa and S. Adachi, J. Appl. Phys. *36*, 6237 (1997).
[2] E. Dumont, B. Dugnoille, and S. Bienfait, Thin Solid Films *353*, 93 (1999).
[3] Z. H. Dai, R. J. Zhang, J. Shao, Y. M. Chen, Y. X. Zheng, J. D. Wu, and L. Y. Chen, J. Korean Phys. Soc. *55*, 1227 (2009).
[4] C.-K. Sun, S.-Z. Sun, K.-H. Lin, K. Y.-J. Zhang, H.-L. Liu, S.-C. Liu, and J.-J. Wu, Appl. Phys. Lett. *87*, 023106 (2005).
[5] H. N. Lin, R. J. Stoner, H. J. Maris, and J. Tauc, J. Appl. Phys. *69*, 3816 (1990).
[6] O. B. Wright, J. Appl. Phys. *71*, 1617 (1992).
[7] H. T. Grahn, D. A. Young, H. J. Maris, J. Tauc, J. M. Hong, and T. P. Smith, Appl. Phys. Lett. *53*, 2023 (1988).
[8] Y.-K. Huang, G.-W. Chern, C.-K. Sun, Y. Smorchkova, S. Keller, U. Mishra, and S. P. DenBaars, Appl. Phys. Lett. *79*, pp. 3361 (2001).
[9] K.-H. Lin, C.-T. Yu, Y.-C. Wen, and C.-K. Sun, Appl. Phys. Lett. *86*, 093110 (2005).
[10] Y.-C. Wen, C.-L. Hsieh, K.-H. Lin, H.-P. Chen, S.-C. Chin, C.-L. Hsiao, Y.-T. Lin, C.-S. Chang, Y.-C. Chang, L.-W. Tu, and C.-K. Sun, Phys. Rev. Lett. *103*, 264301 (2009).
[11] L. P. Martin and M. Rosen, Ultrasonics *35*, 65 (1997).
[12] T. B. Bateman, J. Appl. Phys. *33*, 3309 (1962).
[13] C. Klingshirn, ChemPhysChem. *8*, 782 (2007).
[14] R. J. Elliott, Phys. Rev. *10*, 1384 (1957).
[15] C. Tanguy, IEEE J. Quantum Electron. *32*, 1746 (1996).